

Application of the Gradient Smoothing Technique to the Natural Neighbour Galerkin Method for the Couple-Stress Elasticity

K. Wang¹, S.J. Zhou^{2,3} and Z.F. Nie⁴

Abstract: The natural neighbour Galerkin method is tailored to solve boundary value problems of the couple-stress elasticity to model the size dependent behaviour of materials. This method is based on the displacement-based Galerkin approach, and the calculation of the global stiffness matrix is performed using gradient smoothing technique combined with the non-Sibsonian partition of unity approximation scheme. This method possesses the following properties: the complex C^1 -continuous approximation scheme is avoided without using either Lagrange multipliers or penalty parameters; no domain integrals involved in the assembly of the global stiffness matrix; and the imposition of essential boundary conditions is straightforward. The validity and accuracy of this method are investigated through numerical examples. The results show that strong size effects can be captured by the numerical method when the length of deformation field and the characteristic length of the material are comparable, and good agreements with analytical solutions are obtained.

Keywords: Meshless method, size effect, couple stress, gradient smoothing, natural neighbour interpolation, partition of unity.

1 Introduction

The mechanical behaviour of materials in the micron scale has been experimentally observed to be size dependent [Fleck and Hutchinson (1993); Fleck, Muller, Ashby and Hutchinson (1994); Fleck and Hutchinson (1997)]. Classical continuum theories are unable to explain these phenomena because these theories assume that materials are homogeneous and continuous and there have been no material

¹ Department of Mechanical and Electronic Engineering, JNEVC, Jinan, 250200, P.R.China

² School of Mechanical Engineering, SDU, Jinan 250061, P.R.China

³ Corresponding author. Email: zhousj@sdu.edu.cn

⁴ College of Mechanical and Electronic Engineering ,SDUST, Qingdao 265510, P.R.China

characteristic length quantities in their constitutive equations. In these theories, the stresses at a material point are functions of the strains at the same point, which has been proved to be adequate when the length of deformation field is much larger than the characteristic length of materials. But in the micron scale or dealing with some materials with a granular, fibrous, and cellular structure, where the microstructures of the body are significant, the assumptions of classical theories are questionable. In fact, under these circumstances, the micro-structure of the materials can not be neglected and the stresses at a material point would not only depend on the strains but also on their gradients.

One remedy against the deficiency of the classical theories is to use higher-order theories, e.g. the couple-stress theory [Mindlin and Tiersten (1962); Mindlin (1962)] and the strain gradient theory [Toupin (1962); Mindlin (1964); Fleck and Hutchinson (1997)]. In these theories, the potential energy densities depend on both the strain and strain gradient, which is expressed as the second-order gradient of displacement. As characteristic length quantities are introduced in the constitutive equations, these theories have the abilities to model the size effects phenomenologically. The governing equations of these theories are of fourth order, and the boundary conditions are more complicated. For conventional displacement-based Galerkin approaches, the interpolation of displacement requires C^1 -continuity and second-order completeness in order to ensure the convergence. However, developments of C^1 -continuous elements are so complicated and their performances are not good enough. This drives the developments of various C^0 -continuous elements by using mixed formulations to relax the continuity requirement. Shu, King and Fleck (1999) introduced six isoparametric types of C^0 -continuous elements for the strain gradient theory. The nodal degrees of freedom include nodal displacements and corresponding gradients, and the kinematic relations between them are enforced via the Lagrange multiplier method. Amanatidou and Aravas (2002) also developed C^0 -continuous elements for Mindlin's form I and form III strain gradient formulations [Mindlin (1964)]. Zervos (2008) developed 2D and 3D elements for Form II strain gradient theory using penalty method. From the developments of various mixed methods, we can observe that the use of either Lagrange multipliers or penalty parameters will bring about some side effects. On one hand, the employment of the Lagrange multipliers will introduce additional unknowns, which dramatically expands the scale of the system equations. On the other hand, the use of penalty parameters has some intrinsic disadvantages, e.g. no theoretical criterion available to determine the proper penalty parameter for universal problems. Besides, the approximation schemes for independent field variables should be chosen carefully such that the LBB condition can be satisfied.

In recent years, the so-called meshless methods [Belytschko, Krongauz, Organ,

Fleming and Krysl (1996); Atluri (2004)] were also applied to strain gradient theories. It seems that meshless methods are good at handling such problems. Pamin, Askes and Borst (2003) used element-free Galerkin method (EFG) for the gradient plasticity analysis. Tang, Shen and Atluri (2003) used meshless local Petrov-Galerkin method (MLPG) to solve the boundary value problems of strain gradient elasticity. In Tang's work, the degrees of freedom consist of only nodal displacements, and the MLS is used to generate the displacement approximation space with higher-order continuity and completeness. However, the usage of only nodal displacements may introduce difficulty in imposition of the essential boundary condition of normal derivatives of displacement, which are linear independent of displacements.

The objective of this work is to develop a natural neighbour Galerkin method [Sukumar, Moran, Semenov and Belikov (2001)], which uses relatively low-cost C^0 -continuous meshless approximation scheme, for solving boundary value problems of couple-stress elasticity without using either Lagrange multipliers or penalty parameters. This is realized by two techniques. Firstly, a gradient smoothing operation [Onate and Zarate (2000); Yoo, Moran and Chen (2004); Liu, Nguyen, Dai and Lam (2007); Liu (2008)] is employed within each integration sub-domain, and subsequently the rotation gradients can be expressed as the first-order gradients of displacement, which relaxes the C^1 -continuity requirement. Secondly, the natural neighbour interpolation [Belikov and Semenov (2000)] is enriched with the idea of partition of unity method (PUM) [Babuska and Melenk (1997)] such that the resulting approximation functional space possesses second-order completeness. This enrichment not only gives the approximation the second-order reproducing ability but also enables easy imposition of the essential boundary conditions.

This paper is organized as follows: In section 2, the couple-stress elasticity is briefly reviewed. The application of gradient smoothing technique combined with the non-Sibsonian PUM to the natural neighbour Galerkin method for the couple-stress elasticity is proposed in section 3. In section 4, several numerical examples are presented to investigate the proposed method. This paper ends with the conclusions in section 5.

2 Review of the couple-stress theory

In this section, the couple-stress theory is briefly reviewed. The detailed derivations are skipped, and the reader is referred to the original publication by Mindlin and Tiersten [Mindlin and Tiersten (1962)] or the publications by Fleck and his colleagues [Fleck, Muller, Ashby and Hutchinson (1994); Fleck and Hutchinson (1997)] for details. Tensor index notation is used with the usual summation convention. A comma in the subscript signifies differentiation with respect to the indices

following it.

2.1 Equilibrium equations and boundary conditions

In absence of body forces and body couples, the equilibrium equations and boundary conditions can be written as:

$$\sigma_{ij,j} + \tau_{ij,j} = 0 \text{ in } \Omega \quad (1a)$$

$$\mu_{jk,j} + e_{ijk}\tau_{ij} = 0 \text{ in } \Omega \quad (1b)$$

$$u_i = \bar{u}_i, \quad \theta_i = \bar{\theta}_i \text{ on } \Gamma_u \quad (1c)$$

$$(\sigma_{ij} + \tau_{ij})n_i = \bar{T}_i, \quad \mu_{ij}n_j = \bar{M}_i \text{ on } \Gamma_t \quad (1d)$$

where Ω is the problem domain bounded by the boundary $\Gamma = \Gamma_t + \Gamma_u$, σ_{ij} and τ_{ij} are the symmetric and anti-symmetric parts of the Cauchy stress tensor, μ_{ij} is couple stress tensor, e_{ijk} is the alternating symbol, n_j is the unit outward normal vector to the boundary Γ , \bar{T}_i and \bar{M}_i are the prescribed tractions and couples on the boundary Γ_t , \bar{u}_i and $\bar{\theta}_i$ are prescribed displacements and micro-rotations on the boundary Γ_u , respectively. The couple stress tensor μ_{ij} can be split into its trace part p and its deviatoric part m_{ij} .

$$p = \frac{1}{3}\mu_{ii}, \quad m_{ij} = \mu_{ij} - p\delta_{ij} \quad (2)$$

It was shown that the trace part of the couple stress p does not enter the field equations, and can be assumed to vanish without loss of generality; thus $\mu_{ij} = m_{ij}$. Eq.1a, Eq.1b and Eq.2 can be combined into an alternative form of the equilibrium equation.

$$\sigma_{mn,m} - \frac{1}{2}e_{imn}m_{ji,jm} = 0 \quad (3)$$

2.2 Deformation produced by stress and couple-stress

In the couple-stress theory, it is assumed that the micro-rotation vector θ_i is equal to the macro-rotation vector ω_i represented by the curl of the displacement vector, that is:

$$\theta_i = \omega_i = \frac{1}{2}e_{ijk}u_{k,j} \quad (4)$$

The symmetric strain tensor is the same as that of the classical theory:

$$\varepsilon_{ij} = (u_{i,j} + u_{j,i})/2 \quad (5)$$

And the traceless rotation gradient tensor κ_{ij} is defined as:

$$\kappa_{ij} = \theta_{i,j} = \omega_{i,j} = \frac{1}{2} e_{jkl} u_{l,ki} (\kappa_{ii} = 0) \quad (6)$$

The above equation indicates that the rotation gradient can be expressed as the second-order gradient of displacement. Actually, the rotation gradient accounts for eight components out of eighteen components of the second-order gradient of displacement in 3D. Toupin (1962) and Mindlin (1964) generalized the couple-stress theory to include all the eighteen components of the second-order gradient of displacement. This generalization can be coined as Toupin-Mindlin strain gradient theory or strain gradient theory [Fleck and Hutchinson (1997)].

2.3 Constitutive law

The total deformation energy density depends on both the symmetric strain tensor ε_{ij} and the rotation gradient tensor κ_{ij} . For linear elastic center-symmetric isotropic materials, the potential energy density is defined as [Fleck and Hutchinson (1993)]:

$$w = 2\mu l^2 \kappa_{ij} \kappa_{ij} + \mu \varepsilon_{ij} \varepsilon_{ij} + \frac{1}{2} \lambda \varepsilon_{ii}^2 \quad (7)$$

Where μ and λ are usual Lamé constants, l is the additional characteristic length quantity related to the micro-structure of materials. The symmetric part of Cauchy stress σ_{ij} and couple stress tensor μ_{ij} are work-conjugates with the strain tensor ε_{ij} and the rotation gradient tensor κ_{ij} via the constitutive equations:

$$\sigma_{ij} = \frac{\partial w}{\partial \varepsilon_{ij}} = \lambda \delta_{ij} \varepsilon_{mm} + 2\mu \varepsilon_{ij} \quad (8a)$$

$$\mu_{ij} = \frac{\partial w}{\partial \kappa_{ij}} = 4\mu l^2 \kappa_{ij} \quad (8b)$$

It should be noted there is no work-conjugate with the anti-symmetric part of the Cauchy stress tensor τ_{ij} , so it does not contribute to the internal energy, and therefore τ_{ij} is left indeterminate.

3 The natural neighbour Galerkin method with gradient smoothing technique

3.1 Weak form

For brevity, the functional of potential energy with no body forces and body couples, can be expressed in matrix form by:

$$\begin{aligned} \Pi = & \frac{1}{2} \int_{\Omega} \boldsymbol{\varepsilon}^T \boldsymbol{\sigma} d\Omega + \frac{1}{2} \int_{\Omega} \boldsymbol{\kappa}^T \boldsymbol{\mu} d\Omega \\ & - \int_{\Gamma_t} \mathbf{u}^T \bar{\mathbf{T}} d\Gamma - \int_{\Gamma_t} \boldsymbol{\theta}^T \bar{\mathbf{M}} d\Gamma \end{aligned} \quad (9)$$

By taking the first variation $\delta\Pi = 0$, gives

$$\begin{aligned} & \int_{\Omega} \boldsymbol{\delta\varepsilon}^T \boldsymbol{\sigma} d\Omega + \int_{\Omega} \boldsymbol{\delta\kappa}^T \boldsymbol{\mu} d\Omega \\ & = \int_{\Gamma_t} \boldsymbol{\delta\mathbf{u}}^T \bar{\mathbf{T}} d\Gamma + \int_{\Gamma_t} \boldsymbol{\delta\boldsymbol{\theta}}^T \bar{\mathbf{M}} d\Gamma \end{aligned} \quad (10)$$

Where $\boldsymbol{\delta\varepsilon}$ and $\boldsymbol{\delta\kappa}$ are expressed in terms of $\boldsymbol{\delta\mathbf{u}}$ via

$$\boldsymbol{\delta\varepsilon} = \mathbf{L}\boldsymbol{\delta\mathbf{u}}, \quad \boldsymbol{\delta\kappa} = \mathbf{L}'\boldsymbol{\delta\mathbf{u}} \quad (11)$$

For 2D cases, these matrices are defined as follows:

$$\mathbf{u} = [u_x \quad u_y]^T \quad (12)$$

$$\boldsymbol{\delta\varepsilon} = [\delta\varepsilon_x \quad \delta\varepsilon_y \quad \delta\gamma_{xy}]^T \quad (13a)$$

$$\boldsymbol{\delta\kappa} = [\delta\kappa_x \quad \delta\kappa_y]^T \quad (13b)$$

$$\boldsymbol{\sigma} = [\sigma_x \quad \sigma_y \quad \tau_{xy}]^T \quad (14a)$$

$$\boldsymbol{\mu} = [\mu_x \quad \mu_x]^T \quad (14b)$$

$$\bar{\mathbf{T}} = [\bar{T}_x \quad \bar{T}_y]^T \quad (15a)$$

$$\bar{\mathbf{M}} = [\bar{M}] \quad (15b)$$

$$\mathbf{L} = \begin{bmatrix} \frac{\partial}{\partial x} & 0 & \frac{\partial}{\partial y} \\ 0 & \frac{\partial}{\partial y} & \frac{\partial}{\partial x} \end{bmatrix}^T \quad (16a)$$

$$\mathbf{L}' = \frac{1}{2} \begin{bmatrix} -\frac{\partial^2}{\partial y \partial x} & \frac{\partial^2}{\partial x^2} \\ -\frac{\partial^2}{\partial y^2} & \frac{\partial^2}{\partial x \partial y} \end{bmatrix} \quad (16b)$$

where $\gamma_{xy} = 2\varepsilon_{xy}$ is the shear strain.

3.2 Integration scheme for domain integrals

The evaluation of the integrals over global domain in Eq.10 could be carried out on the Delaunay triangles ($T_i, i=1, \dots, m$). The second domain integral of l.h.s. of the Eq.10 includes second-order gradient of displacement. In order to evaluate it, a C^1 -continuous approximation scheme should be used to make the integral integrable. However, construction of a C^1 -continuous interpolation needs much more effort and increases the computational costs. If we want to relax the continuity requirement, the order of the integrand should be reduced. Onate and Zarate (2000) developed rotation-free triangular plate and shell elements by incorporating the finite volume method. In their work, the curvature within each control domain, is assumed to be constant and can be expressed as the first-order gradient of displacement. Consequently, the domain integrals are transformed into line integrals and the order of the integrand is reduced. Motivated by their work, we could relax the continuity requirement by following this strategy.

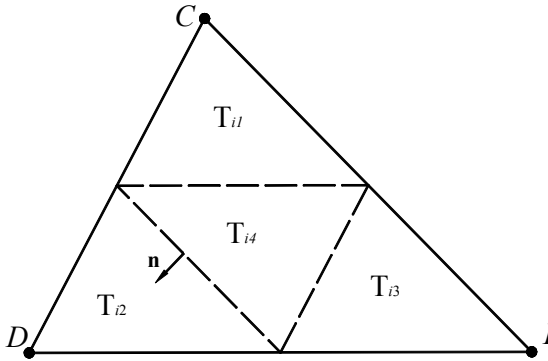


Figure 1: Sub-division of the Delaunay triangle

Firstly, we decompose each Delaunay triangle, e.g. ΔIDC in Fig.1, into four identical small triangles by connecting the mid-points of its edges. The k th sub-triangle in the i th Delaunay triangle is denoted by T_{ik} . By considering the constitutive relation, the second domain integral of l.h.s. of the Eq.10 could be evaluated as

$$\int_{T_i} (\mathbf{L}' \delta \mathbf{u})^T \boldsymbol{\mu} d\Omega = \sum_{k=1}^4 \left(\int_{T_{ik}} (\mathbf{L}' \delta \mathbf{u})^T \mathbf{D}' \boldsymbol{\kappa} d\Omega \right) \quad (17)$$

Where \mathbf{D}' is the constitutive matrix defined by

$$\mathbf{D}' = \begin{bmatrix} 4\mu l^2 & 0 \\ 0 & 4\mu l^2 \end{bmatrix} \quad (18)$$

Secondly, over each integration sub-domain T_{ik} , the gradient smoothing technique [Yoo, Moran and Chen (2004); Liu, Nguyen, Dai and Lam (2007); Liu (2008)] is adopted, and the constant rotation gradient field is defined as a weighted average (non-local curvature):

$$\tilde{\boldsymbol{\kappa}} = \int_{T_{ik}} \mathbf{L}' \mathbf{u} \phi(x) d\Omega \quad (19)$$

The smoothing function $\phi(x)$ satisfies at least the unity property:

$$\int_{T_{ik}} \phi(x) d\Omega = 1 \quad (20)$$

Here, the following constant smoothing function is used:

$$\phi(x) = \begin{cases} \frac{1}{A_{ik}} & \text{if } x \in T_{ik} \\ 0 & \text{if } x \notin T_{ik} \end{cases} \quad (21)$$

Where A_{ik} is the area of T_{ik} . Using divergence theorem, Eq.19 becomes:

$$\tilde{\boldsymbol{\kappa}} = \frac{1}{A_{ik}} \int_{\partial T_{ik}} \mathbf{N}' \nabla' \mathbf{u} d\Gamma \quad (22)$$

where

$$\mathbf{N}' = [n_x \quad n_y]^T, \quad \nabla' = \frac{1}{2} \begin{bmatrix} -\frac{\partial}{\partial y} & \frac{\partial}{\partial x} \end{bmatrix} \quad (23)$$

By Eq.22, the constant rotation gradient field is defined, i.e. $\boldsymbol{\kappa} \doteq \tilde{\boldsymbol{\kappa}}$, within each integration sub-domain T_{ik} . Thus, Eq.17 can be expressed as:

$$\begin{aligned} & \int_{T_i} (\mathbf{L}' \delta \mathbf{u})^T \boldsymbol{\mu} d\Omega \\ &= \sum_{k=1}^4 \left\{ \left[\int_{T_{ik}} (\mathbf{L}' \delta \mathbf{u})^T d\Omega \right] \mathbf{D}' \tilde{\boldsymbol{\kappa}} \right\} \end{aligned} \quad (24)$$

Integrating by parts the domain integral in the r.h.s of Eq.24 and substituting Eq.22 into it, gives

$$\begin{aligned} & \int_{T_i} (\mathbf{L}' \delta \mathbf{u})^T \boldsymbol{\mu} d\Omega \\ &= \sum_{k=1}^4 \left\{ \left[\int_{\partial T_{ik}} (\mathbf{N}' \nabla' \delta \mathbf{u})^T d\Gamma \right] \mathbf{D}' \left(\frac{1}{A_{ik}} \int_{\partial T_{ik}} \mathbf{N}' \nabla' \mathbf{u} d\Gamma \right) \right\} \end{aligned} \quad (25)$$

The r.h.s of Eq.25 includes only the first-order gradients of displacements, and therefore the C^0 -continuous interpolation could be used to evaluate it.

As to the first domain integral of Eq.10, although it can be evaluated by the usual procedure [Sukumar, Moran, Semenov and Belikov (2001); Sukumar, Moran and Belytschko (1998)], it is reported that the usage of the gradient smoothing operation can obtain more accurate results and higher convergence rate without increasing computational cost [Liu, Nguyen, Dai and Lam (2007); Liu(2008)]. Therefore, we adopt the same operation to improve the accuracy and construct a uniform code structure. Similarly, the first integral over the global domain can be expressed as:

$$\begin{aligned} & \int_{T_i} (\mathbf{L}\delta\mathbf{u})^T \boldsymbol{\sigma} d\Omega \\ &= \sum_{k=1}^4 \left\{ \left[\int_{\partial T_{ik}} (\mathbf{N}\delta\mathbf{u})^T d\Gamma \right] \mathbf{D} \left(\frac{1}{A_{ik}} \int_{\partial T_{ik}} \mathbf{N}\mathbf{u} d\Gamma \right) \right\} \end{aligned} \quad (26)$$

Where \mathbf{D} is the usual elastic constitutive matrix and \mathbf{N} is the matrix defined by:

$$\mathbf{N} = \begin{bmatrix} n_x & 0 & n_y \\ 0 & n_y & n_x \end{bmatrix}^T \quad (27)$$

3.3 The non-Sibsonian partion of unity method

The non-Sibsonian interpolation [Sukumar, Moran, Semenov and Belikov (2001); Belikov and Semenov (2000)] is a kind of the so-called natural neighbor interpolations based on the Voronoi diagram of the scattered nodes. The non-Sibsonian interpolation shape function $\varphi_I(x)$ is calculated by:

$$\varphi_I(\mathbf{x}) = \frac{s_I(\mathbf{x})/h_I(\mathbf{x})}{\sum_{J=1}^n [s_J(\mathbf{x})/h_J(\mathbf{x})]} \quad (28)$$

Where n is the number of natural neighbours of the point \mathbf{x} , s_I is the Lebesgue measure of the Voronoi boundary associated with node I (here is the length of Voronoi edge in 2D case), and h_I is the distance between the evaluated point \mathbf{x} and the node I . This kind of interpolation shares many properties with the Sibson interpolation [Sukumar, Moran and Belytschko (1998)], e.g. linear completeness, partition of unity and the Kronecker Delta property, and is less computationally expensive. However, this interpolation scheme only has linear completeness and C^0 -continuity at the node, which restricts its applications to the couple-stress elasticity. Although, a C^1 -continuous natural neighbour interpolation shape function which has second-order completeness can be constructed [Sukumar and Moran (1999)], the more efficient way to increase the completeness is to enrich the natural neighbour interpolation using the idea of PUM. The PUM can be viewed as a generalized framework to

construct proper approximation spaces with any desired completeness or including any prior knowledges for solving partial differential equations. The approximation schemes used in meshless methods or finite element methods can be considered as special cases of the PUM. Many researchers [Duarte, Babuska, and Oden (2000); Fan, Liu and Lee (2004); Wells, Sluys and De Borst (2002)] have used the PUM to enrich the interpolation extrinsically in Galerkin methods. Gonzalez, Cueto and Doblare (2004) used the PUM to enrich the non-Sibsonian interpolation with polynomial basis in the mixed approximation to verify the LBB condition.

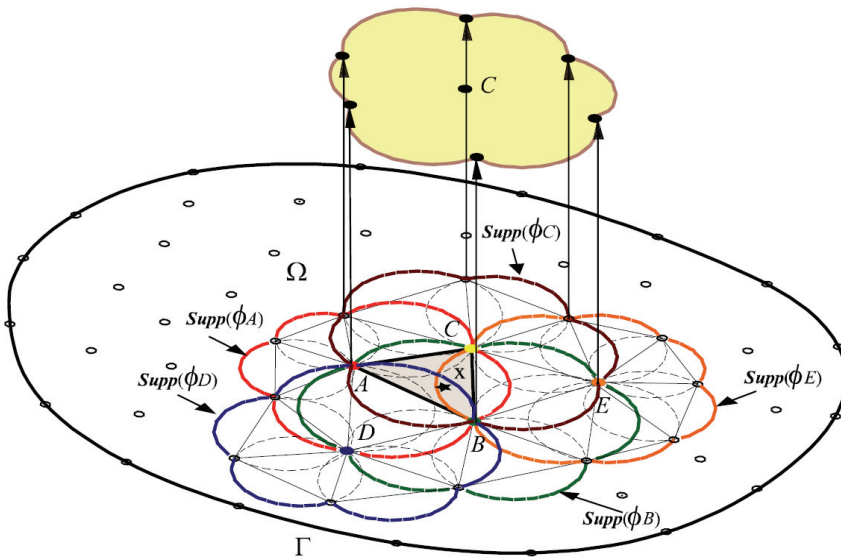


Figure 2: Overlapping patches contributing to the evaluating point x in the NSPU approximation

As the non-Sibsonian interpolation shape function has the property of partition of unity, we can use it to construct an approximation space of second-order completeness which combines features of the non-Sibsonian interpolation shape function. This approximation scheme can be called the non-Sibsonian partition of unity (NSPU). In the NSPU, the problem domain is covered by overlapped patches, as shown in Fig.2. Each patch coincides with the support of the nodal non-Sibsonian shape function $\varphi_I(\mathbf{x})$, and therefore there is a one-to-one corresponding relationship between each patch and each node. On each patch, a local approximation space V_I , also known as the cover function, is constructed by a linear combination

of the influence function ψ_{IJ} [Fan, Liu and Lee (2004)]

$$V_I(\mathbf{x}) = \sum_{J=1}^m a_{IJ} \psi_{IJ}(\mathbf{x}) \quad (29)$$

Then the global approximation space V is constructed by

$$V(\mathbf{x}) = \sum_{I=1}^n \varphi_I(\mathbf{x}) V_I(\mathbf{x}) \quad (30)$$

Where n is the number of natural neighbours of the evaluating point \mathbf{x} . This is different from the general PUM where all nodes, be it near or far, will contribute a share to the total sum at an arbitrary location. For example, in Fig.2, the evaluating point \mathbf{x} has five natural neighbours, i.e. A, B, C, D and E , and a typical patch of node C is illustrated. These five patches cover the evaluating point \mathbf{x} . Only the local approximation spaces defined on these patches contribute to the evaluating point, and the nodal non-Sibsonian shape function $\varphi_I(\mathbf{x})$ defines the percentage contribution from the node I 's patch. This ensures the local property of the approximation and a subsequent compact banded stiffness matrix. As the important property of the PUM is that the global approximation space V inherits the approximation properties of the local space V_I and the smooth of the partition of unity, the resultant non-Sibsonian PU approximation scheme remains C^0 -continuity.

The influence function ψ_{IJ} can be chosen with great flexibility. The most straightforward choice is polynomial functions [Duarte, Babuska and Oden (2000)]. It is worth noting that different influence functions could be used for different patches. While, adopting a single repetitive type of influence function is quite convenient here. In order to achieve the second-order completeness, the polynomials $\{1, x, y\}$ is used to construct the local cover function V_I [Gonzalez, Cueto and Doblare (2004)], such that the resultant approximation is

$$\Phi = \varphi_I \times \{1, x, y\}, \quad I = 1, \dots, n \quad (31)$$

As non-Sibsonian interpolation shape function has the linear completeness, there exist constants a_I^x and $a_I^y, I = 1, \dots, n$, such that

$$\sum_{I=1}^n \varphi_I = 1, \quad \sum_{I=1}^n \varphi_I a_I^x = x, \quad \sum_{I=1}^n \varphi_I a_I^y = y \quad (32)$$

From the above equations, we have [Duarte, Babuska and Oden (2000)]

$$\sum_{I=1}^n (\varphi_I x) a_I^x = x \sum_{I=1}^n \varphi_I a_I^x = x^2 \quad (33a)$$

$$\sum_{I=1}^n (\varphi_I x) a_I^y = x \sum_{I=1}^n \varphi_I a_I^y = xy \quad (33b)$$

$$\sum_{I=1}^n (\varphi_I y) a_I^y = y \sum_{I=1}^n \varphi_I a_I^y = y^2 \quad (33c)$$

$$\sum_{I=1}^n (\varphi_I y) a_I^x = y \sum_{I=1}^n \varphi_I a_I^x = yx \quad (33d)$$

Therefore, it can be concluded that

$$\text{span}\{\Phi\} = \text{span}\{1, x, y, xy, x^2, y^2\} \quad (34)$$

In the numerical implementation, setting the origin of the local polynomial enrichment to the node being enriched ensures a well-conditioned system irrespective of the global dimensions [Wells, Sluys and De Borst (2002)]. Thus, the local approximation is calculated by

$$V_I = a_{I1}(x - x_I) + a_{I2}(y - y_I) + a_{I3} \quad (35)$$

By using the above NSPU, the displacement field over a volume can be interpolated by

$$u^h(\mathbf{x}) = \sum_{I=1}^n \varphi_I [a_{I1}(x - x_I) + a_{I2}(y - y_I) + a_{I3}] \quad (36)$$

The above equation can also be written as

$$\begin{aligned} u^h(\mathbf{x}) &= \sum_{I=1}^n \varphi_I a_{I3} \\ &+ \sum_{I=1}^n [\varphi_I(x - x_I)a_{I1} + \varphi_I(y - y_I)a_{I2}] \end{aligned} \quad (37)$$

In above equation, the first part of the r.h.s can be viewed as the conventional non-Sibsonian interpolation, and the second part is the enrichment. In 2D problems, the displacement vector has two components, that is

$$\mathbf{u} = [u_x \quad u_y]^T = \sum_{I=1}^n \phi_I \hat{\mathbf{u}}_I \quad (38)$$

where

$$\phi_I = \begin{bmatrix} \varphi_{I1} & \varphi_{I2} & \varphi_{I3} & 0 & 0 & 0 \\ 0 & 0 & 0 & \varphi_{I1} & \varphi_{I2} & \varphi_{I3} \end{bmatrix} \quad (39)$$

$$\hat{\mathbf{u}}_I = [a_{I1}^x \quad a_{I2}^x \quad a_{I3}^x \quad a_{I1}^y \quad a_{I2}^y \quad a_{I3}^y]^T \quad (40)$$

Where $\varphi_{I1} = \varphi_I(x - x_I)$, $\varphi_{I2} = \varphi_I(y - y_I)$ and $\varphi_{I3} = \varphi_I$ are defined for simplicity, and the $\hat{\mathbf{u}}_I$ is the column vector containing the generalized nodal parameters. When the evaluating point \mathbf{x} reaches the node, e.g. \mathbf{x}_I , because of the Kronecker Delta property of the non-Sibsonian shape function, i.e. $\varphi_I(\mathbf{x}_J) = \delta_{IJ}$, the displacement $u^h(\mathbf{x})$ will only depends on the local approximation defined on the node I 's patch, and therefore

$$u^h(\mathbf{x}_I) = a_{I1}(x_I - x_I) + a_{I2}(y_I - y_I) + a_{I3} = a_{I3} \quad (41)$$

Therefore, the components a_{I3}^x and a_{I3}^y can be considered as the ‘‘regular’’ nodal degrees of freedom of displacements and the other four parameters can be considered as their spatial derivatives approximately. This is quite similar with the C^1 natural neighbour interpolation [Sukumar and Moran (1999)], and facilitates the imposition of essential boundary condition for the couple-stress and strain gradient theories. It is worth noting that either setting all influence functions to unity or setting the enriched nodal parameters to zero will reduces the NSPU to the tradition non-Sibsonian interpolation.

3.4 Discrete form and numerical implementation

By substituting Eq.38 into Eq.25 and Eq.26 and subsequently into Eq.10, the matrix form of discrete equations can be expressed by:

$$\mathbf{K}_{6N \times 6N} \hat{\mathbf{u}}_{6N} = \mathbf{F}_{6N} \quad (42)$$

$$\mathbf{K}_{IJ} = \sum_{i=1}^m \sum_{k=1}^4 \left(\mathbf{B}_I^T \mathbf{D} \mathbf{B}_J + \mathbf{B}'_I{}^T \mathbf{D}' \mathbf{B}'_J \right) A_{ik} \quad (43)$$

$$\mathbf{F}_I = \int_{\Gamma_I} \boldsymbol{\phi}_I^T \bar{\mathbf{T}} d\Gamma + \int_{\Gamma_I} (\nabla' \boldsymbol{\phi}_I)^T \bar{\mathbf{M}} d\Gamma \quad (44)$$

Where N denotes the total number of nodes placed on the boundary and in the domain. The matrices included in above equations, e.g. \mathbf{B}_I and \mathbf{B}'_I , are defined by

$$\mathbf{B}_I = \frac{1}{A_{ik}} \int_{\partial T_{ik}} \mathbf{N} \boldsymbol{\phi}_I d\Gamma \quad (45)$$

$$\mathbf{B}'_I = \frac{1}{A_{ik}} \int_{\partial T_{ik}} \mathbf{N}' \nabla' \boldsymbol{\phi}_I d\Gamma \quad (46)$$

The pseudo code shown in Tab. 1 can be used to construct the global stiffness matrix. Obviously, the assembly of the stiffness matrix here is quite different from that

of the original natural neighbour Galerkin method. There are no domain integrals involved in the calculation of the stiffness matrix. However, the line integrations involved in the matrix \mathbf{B}_I and \mathbf{B}'_I would influence the result greatly. It is reported that the application of the trapezoidal quadrature rule to the line integrals might cause problems. Instead, the employment of the Gaussian quadrature rule proves to be suit with the properties of the non-Sibsonian interpolation [Yoo, Moran and Chen (2004)]. In our work, one Gaussian points per interior segment and two Gaussian points per boundary segment are used. This provides the ease of weight computation for interior segment, as the weight is the length of the segment itself.

Table 1: The pseudo code for assembly of the global stiffness matrix

Loop over all the Delaunay triangles ($i=1, m$)
Loop over the sub-triangles of each Delaunay triangle ($k=1, 4$)
Loop over three edges of each sub-divided small triangle ($l=1, 3$)
Calculate the length and out normal vector of the edge
Loop over Gaussian points on the edge
Calculate the corresponding weight of the Gaussian point
Calculate the non-Sibsonian interpolation shape function and its derivatives
Loop over the natural neighbours ($l=1, n$)
Set a mark on the natural neighbours nodes
Calculate and assemble the contribution to the matrices \mathbf{B}_I and \mathbf{B}'_I
End loop over the natural neighbours
End loop over Gaussian Points
End loop over three edges
Count the number of natural neighbours involved in the line integration on the three edges of the small triangle with the aid of the marks
Loop over the natural neighbours I
Loop over the natural neighbours J
Calculate $(\mathbf{B}_I^T \mathbf{D} \mathbf{B}_J + \mathbf{B}'_I{}^T \mathbf{D}' \mathbf{B}'_J) A_{lk}$ and add it to the global stiffness matrix
End loop over the natural neighbours J
End loop over the natural neighbour I
End loop over the sub-divided small triangles
End loop over the Delaunay triangles

4 Numerical examples

In order to test the performance of the proposed numerical method and observe its ability of modelling the size effect, three numerical examples having analytical solutions are presented. In all the examples, the geometric dimensions are fixed and the material length is varied in order to observe the size effect easily. In the last example, we follow Cordes and Moran (1996) to treat the material discontinuity. The material interface is modeled by a set of nodes that belong to both materials. Any points contained in the material #1 can only be influenced by nodes in material #1 plus the interface nodes and vice versa.

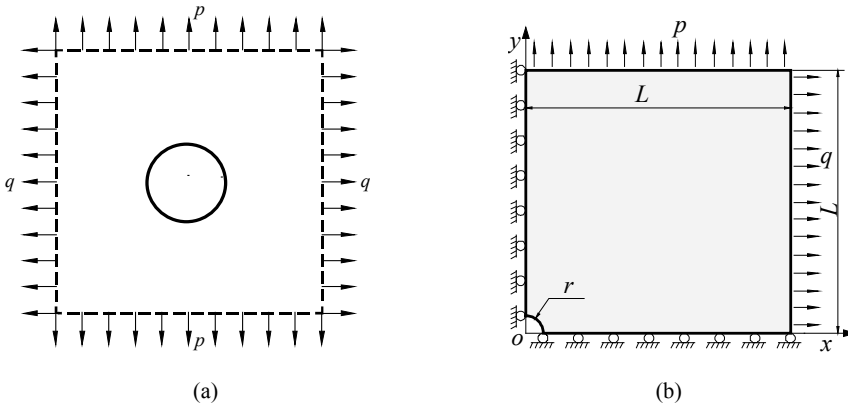


Figure 3: Square with hole in a field of biaxial tension

4.1 Square with hole under biaxial tensions

An infinite square plate with a centric circular hole under biaxial tension is illustrated in Fig.3a. According to the work by Mindlin (1963), couple stresses have no effect at all on the stresses around a circular hole when p is equal to q . When p equals to zero, this problem becomes the uniaxial tension, the maximum normal stress in the vicinity of the hole will be reduced due to the effect of couple stresses. If p equals q in magnitude but have opposite signs, i.e. $p=-q$, the other extreme case of pure shear occurs and the effect of couple stresses is even greater than that of the uniaxial tension. In this example, we will deal with the latter two extreme cases. The analytical solution for stresses, couple stresses and the stress concentration factor of this problem are given by Mindlin (1962).

Due to symmetry, only the upper right quadrant of the plate is modeled as shown in Fig.3(b). The length of the plate L and the radius of the hole r are chosen to be 7.5 and 0.5, respectively. As the ratio of L to r is 15, the plate can be approximately considered as infinite. Symmetric conditions are imposed on the left and bottom boundaries, where the micro-rotation $\theta = 0$ is also set. The traction boundary conditions are set as follow:

For the uniaxial tension problem

- On the right boundary: $T_x = q=1.0$, $T_y = M=0.0$
- On the top boundary: $T_x = T_y = M=0.0$

For the pure shear problem

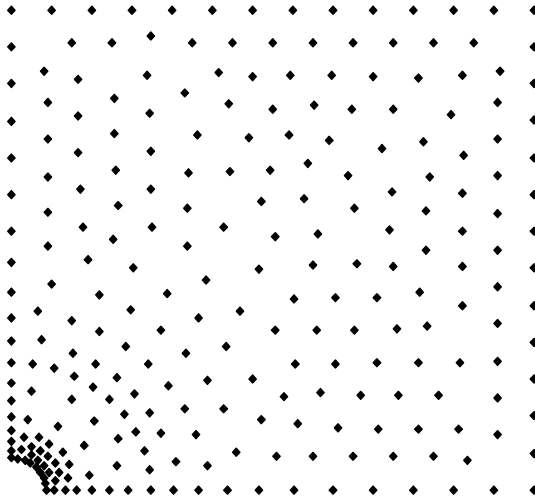


Figure 4: The discrete model with 259 irregular nodes

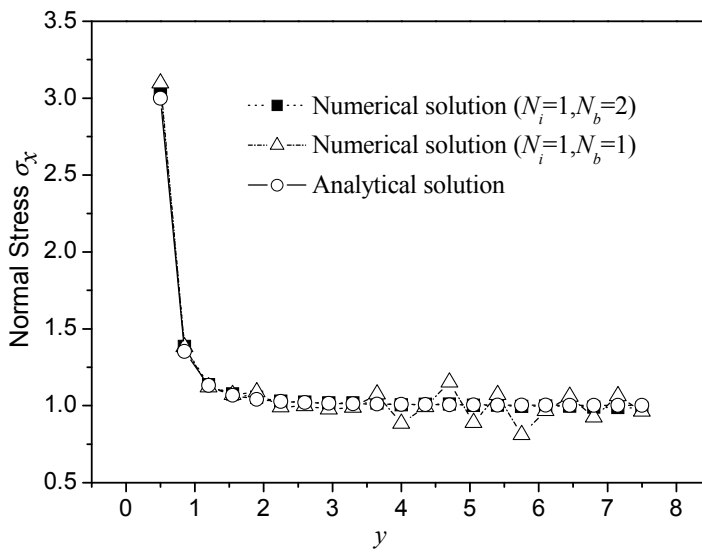


Figure 5: Normal stress σ_x along left edge at $x = 0$

- On the right boundary: $T_x = q = 1.0$, $T_y = 0.0$
- On the top boundary: $T_x = 0.0$, $T_y = p = -1.0$

In the numerical computation, the plane stress condition is assumed with material constants $E=1.0$ and $\nu=0.3$. Irregular nodal arrangement with only 259 nodes shown in Fig.4 is used.

When the material length $l=0.0$ is taken, the ratio of the radius of the hole r to the material length l approaches infinity. As we can predict, the couple stresses can be neglected and the classical theory will be reproduced. First, we test the influence of the number of integration points on the accuracy of the solution. This can be observed from the Fig.5, where the normal stress σ_x along left edge at $x=0$ for the case $l=0.0$ is plotted. If one Gaussian point for both interior and the boundary segment are used ($N_i=1, N_b=1$), the oscillatory solution is obtained (although, the usage of much more nodes will give some remedy for this). On the contrary, stable and accurate solution is obtained using one Gaussian point per interior segment and two Gaussian points per boundary segment ($N_i=1, N_b=2$).

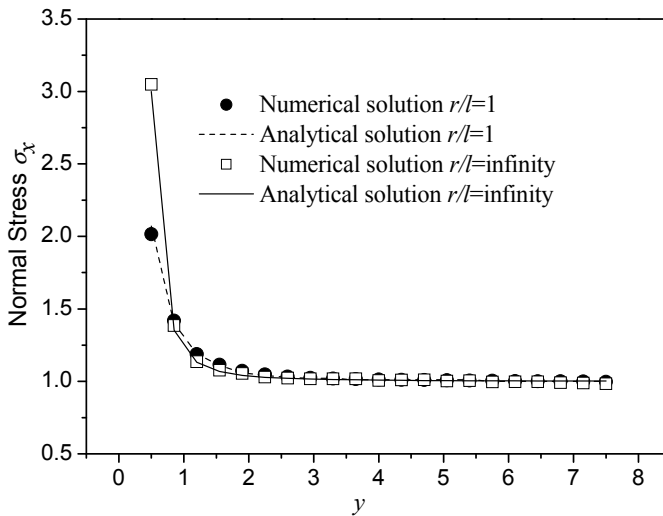


Figure 6: Normal stress σ_x along left edge at $x = 0$

In Fig.6, the comparison between solutions for $l=0.0$ and $l=0.5$ is presented. Due to the existence of the couple stress, the normal stress σ_x in the vicinity of the hole is lowered and the stress concentration factor is reduced to 2.07 for the uniaxial tension. The numerical and analytical solutions are matched quite well. It is known

that the stress concentration factor depends on both Poisson's ratio and the ratio of the radius of the hole r to the material length l [Mindlin (1962)]. In Tab.2 and Tab.3, the stress concentration factors for uniaxial tension and pure shear problems are shown, respectively, for a range of r/l and with different Poisson's ratio. From these two tables, we can observe that as r/l increases, the stress concentration factors increase as well. When r/l approaches infinity, the obtained stress concentration factors will approach the usual value 3.0 for the uniaxial tension and 4.0 for the pure shear problem.

Table 2: Stress concentration factor: $V=0.3$

r/l	Uniaxial tension			Pure shear		
	Analytical	Numerical	% error	Analytical	Numerical	% error
0.5	1.9239	1.8845	2.05	1.8478	1.7664	4.41
1.0	2.0666	2.0159	2.45	2.1332	2.0129	5.64
2.0	2.3356	2.3082	1.17	2.6712	2.5422	4.83
4.0	2.6580	2.6844	0.99	3.3161	3.2367	2.39
5.0	2.7439	2.7861	1.54	3.4877	3.4263	1.76
8.0	2.8737	2.9362	2.17	3.7474	3.7066	1.09
10.0	2.9129	2.9790	2.27	3.8259	3.7863	1.04
100	2.9989	3.0532	1.81	3.9978	3.9210	1.92

Table 3: Stress concentration factor: $V=0.4999$

r/l	Uniaxial tension			Pure shear		
	Analytical	Numerical	% error	Analytical	Numerical	% error
0.5	2.0916	1.9544	6.56	2.1833	1.8617	14.73
1.0	2.2305	2.0856	6.50	2.4612	2.1340	13.29
2.0	2.4755	2.3913	3.40	2.9512	2.6789	9.23
4.0	2.7431	2.7660	0.83	3.4863	3.3666	3.43
5.0	2.8100	2.8626	1.87	3.6201	3.5475	2.01
8.0	2.9081	2.9973	3.07	3.8162	3.8034	0.34
10.0	2.9370	3.0323	3.24	3.8741	3.8711	0.08
100	2.9992	3.0782	2.63	3.9984	3.9718	0.67

4.2 Simple shear problem

Consider a block of width w , length L , and height H undergoing a simple shear deformation, as shown in Fig.7. Assume that w and L are much larger than H such

that they both can be viewed as infinite. The displacement $\bar{u}_x=1.0$ is prescribed on the top surface $y = H$. The analytical solution to this problem is given in the reference [Yang, Chong, Lam and Tong (2002)].

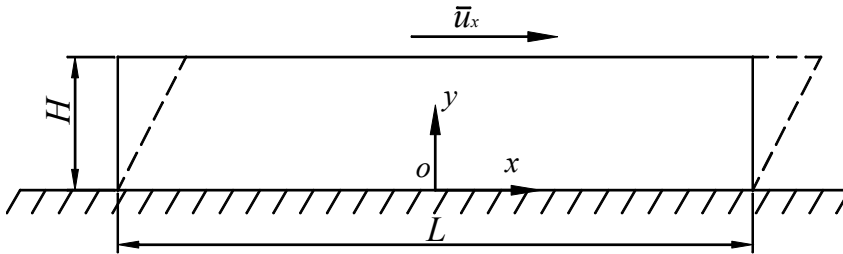


Figure 7: Simple shear problem

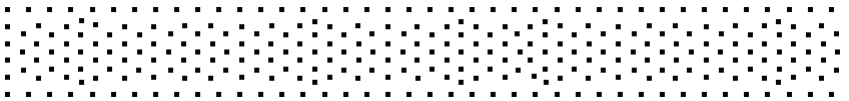


Figure 8: Nodal arrangement for the simple shear problem.

In the computation, the length and the height of the block are taken to be $L=10.0$ and $H=1.0$. The plane strain condition is assumed with material parameters $E = 1.0$ and $\nu=0.3$. The irregular nodal arrangement with 299 nodes shown in Fig.8 is used. The numerical solutions of displacement and shear strain along y -axis at $x=0$ against the analytical ones for different material lengths are plotted in the Fig.9 and Fig.10. We can observe that the numerical solution reduced to the classical solution when the material length vanished. When the material length l and the length of the deformation field H can be comparable, strong size effects was captured by the numerical solution. In both situations, numerical and analytical solutions are matched very well.

4.3 Boundary layer near a bimaterial interface

The couple-stress theory predicts the existence of boundary layers (BL) adjacent to certain types of boundaries such as material interfaces [Fleck and Hutchinson (1993)]. In this test, we consider an interface between two elastic solids under a

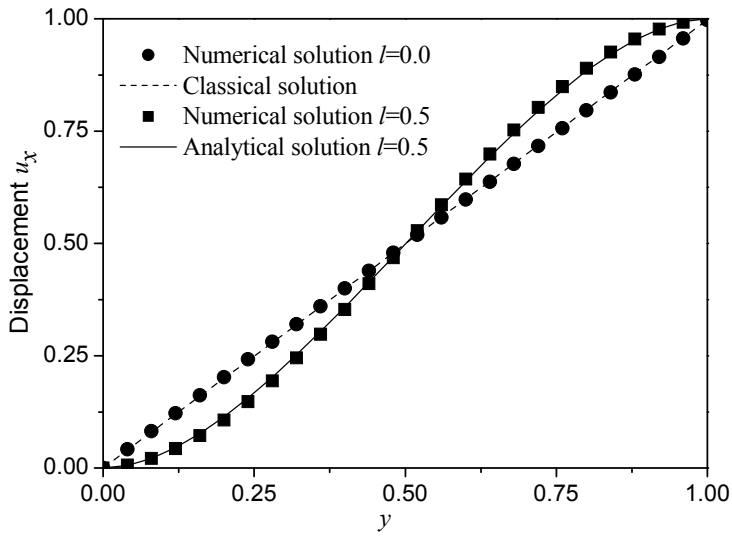


Figure 9: Nodal arrangement for the simple shear problem.

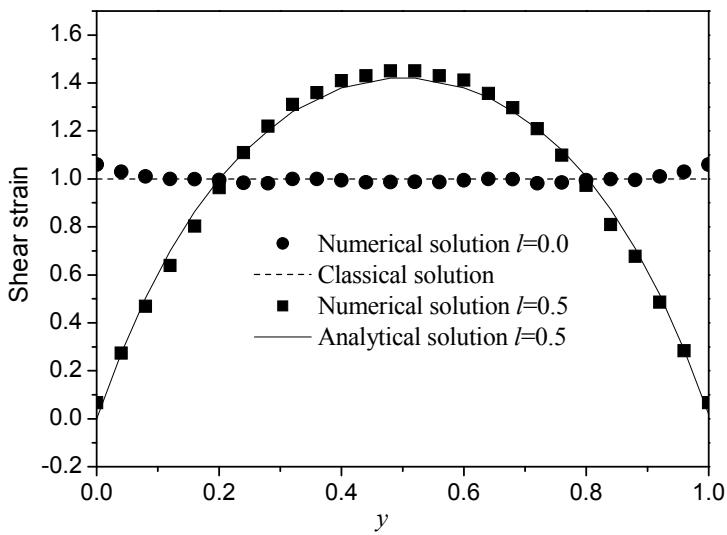


Figure 10: Shear strain $\gamma = 2\epsilon_{xy}$ in the block.

remote shear stress $\sigma_{yx}^\infty = 1.0$ as shown in Fig.11a. If the length of deformation field is comparable with the material length, according to the couple-stress theory, the shear strain $\gamma = 2\varepsilon_{xy}$ has a continuous but non-uniform distribution within a boundary layer adjacent to the interface. The analytical solution of shear strain to this problem is given in the paper of Fleck and Hutchinson (1993).

$$\gamma = \frac{\sigma_{yx}^\infty}{G_1} \left\{ 1 + \frac{G_1 - G_2}{G_2} \cdot \frac{G_2 l_2}{G_1 l_1 + G_2 l_2} \cdot e^{y/l_1} \right\} \text{ for } y < 0$$

$$\gamma = \frac{\sigma_{yx}^\infty}{G_2} \left\{ 1 + \frac{G_2 - G_1}{G_1} \cdot \frac{G_1 l_1}{G_1 l_1 + G_2 l_2} \cdot e^{-y/l_2} \right\} \text{ for } y > 0$$
(47)

Where $G_i = E_i/2(1 + \nu_i)$ is the shear modulus. In order to normalize the solution in dimensionless form, we define the average shear strain as

$$\bar{\gamma} = \sigma_{yx}^\infty (G_1 + G_2) / (G_1 G_2)$$
(48)

The normalized shear strain is defined as the ratio of γ to $\bar{\gamma}$.

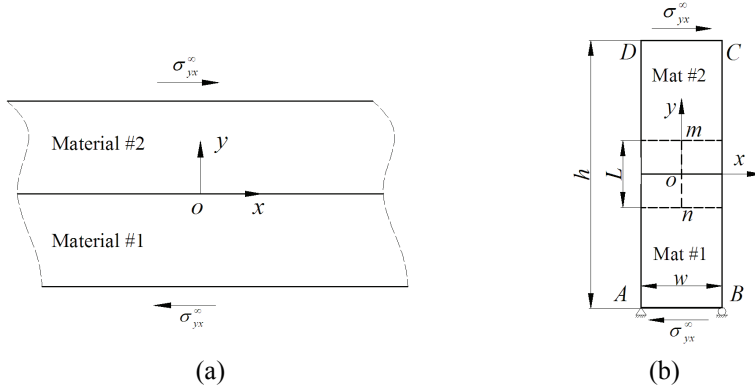


Figure 11: (a) The bimaterial under a remote shear stress and (b) The analytical model

In the numerical computation, the material constants are arbitrarily chosen to be $E_1=2E_2=2.0$, $l_1 = l_2 = l$ and $\nu_1 = \nu_2 = 0.3$. The material length l is taken to be 0.0, 1.0 and 2.0 to observe the size effect. This problem is modeled as shown in the Fig.11b. The width w and the height h of the model are chosen to be $w=1.0$ and $h=50.0$ to represent the dimensional infinity. A central region of length $L=20.0$ is used to simulate the BL. The $u_x = u_y=0$ is set at the left-bottom corner A and $u_y=0$ at

the right-bottom corner B to avoid the rigid movement, and besides, the following boundary condition are prescribed.

On the left boundary AD : $T_x = T_y = M = u_y = \theta = 0$

On the right boundary BC : $T_x = T_y = M = u_y = \theta = 0$

On the bottom boundary AB : $T_x = -\sigma_{yx}^\infty, T_y = M = 0$

On the top boundary DC : $T_x = \sigma_{yx}^\infty, T_y = M = 0$

In the Fig.12, the discrete model consisting of 280 nodes is used in the computation. The discrete model is scaled and rotated 90 degree for illustration purpose. There are 4×31 regular nodes placed on the BL, and 156 irregular nodes arbitrarily placed on the remaining part.

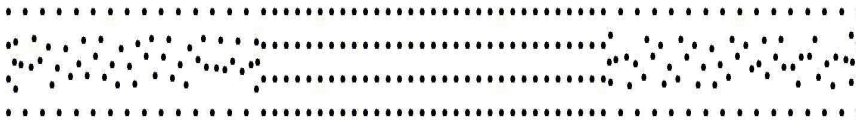


Figure 12: Nodal arrangement with 280 nodes

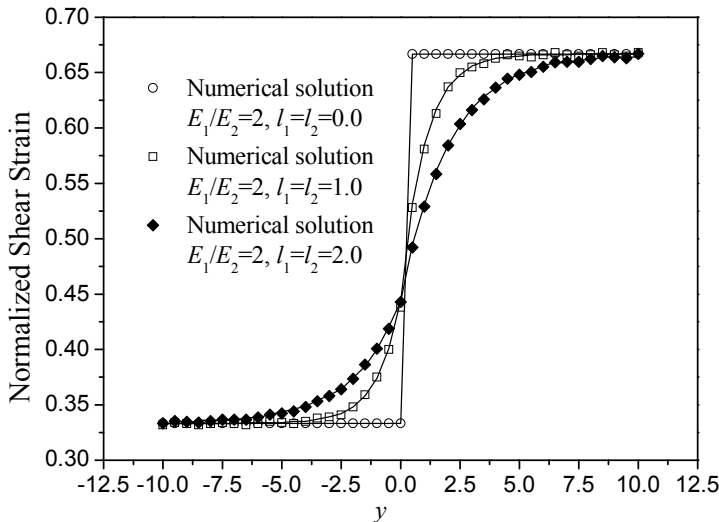


Figure 13: The normalized shear strain

The numerical solutions of the normalized shear strains along line mn against the analytical ones are shown in the Fig.13, where the solid lines denote the analytical solutions and the scattered points denote the numerical solutions. Perfect matches are observed for all the three cases even though only 280 nodes are used. From this figure, we can observe that the shear strain jumps in magnitude at the interface, from $\sigma_{yx}^{\infty}/(\bar{\gamma}G_1) = 0.333$ in material #1, to $\sigma_{yx}^{\infty}/(\bar{\gamma}G_2) = 0.667$ in material #2 when material length l vanishes, which is coincident with the classical solution. When the material length and the length of the deformation field is comparable, the couple stress solutions of the shear strain for $l=1.0$ and $l=2.0$ at the interface are continuous. It also indicates from the figure that the larger the material length is the smaller slope of the distribution can be observed.

5 Conclusions

The gradient smoothing technique combined with the non-Sibsonina PUM is used to tailor the natural neighbour Galerkin method for the couple-stress elasticity to model the size dependent behaviour of materials. Although, the proposed numerical method only considers eight components of the second-order gradient of displacement, the generalization of the proposed method to the strain gradient theory is straightforward. By virtue of the techniques adopted in this method, the domain integrals are transformed into line integrals and the order of integrands are reduced. As a result, this method possesses the following properties: The complicated C^1 -continuous approximation scheme is avoided without using either Lagrange multipliers or penalty parameters; the non-Sibsonian partition of unity is used to construct approximation space with second-order completeness, and therefore the imposition of essential boundary conditions is straightforward; no domain integrals involved in the assembly of the global stiffness matrix. The validity and accuracy of the proposed method are investigated through numerical examples. The numerical results indicate: the classical solutions will be reproduced when the material length quantities are omitted; On the contrary, strong size effects can be observed when the length of deformation field and the material length are comparable. In all tests, good agreements with analytical solutions are obtained.

Acknowledgement: The authors would like to acknowledge the support of the National Natural Science Foundation of China (10572077) and the Chinese Ministry of Education University Doctoral Research Fund (20060422013).

References

- Fleck, N. A.; Hutchinson, J. W.** (1993): A phenomenological theory for strain gradient effects in plasticity. *J. Mech. Phys. Solids*, vol. 41, no. 12, pp. 1825–1857.
- Fleck, N. A.; Muller, G. M.; Ashby, M. F.; Hutchinson, J. W.** (1994): Strain gradient plasticity: theory and experiment. *Acta Metall. Mater.*, vol. 42, no. 2, pp. 475–487.
- Fleck, N. A.; Hutchinson, J. W.** (1997): Strain gradient plasticity. *Adv. Appl. Mech.*, vol. 33, pp. 295–361.
- Mindlin, R. D.; Tiersten, H. F.** (1962): Effects of couple stresses in linear elasticity. *Arch. Rational. Mech. Anal.*, vol. 11, no. 1, pp. 415–448.
- Mindlin, R. D.** (1962): Influence of couple-stresses on stress concentrations. *Exp. Mech.* vol. 3, no. 1, pp. 1–7.
- Toupin, R. A.** (1962): Elastic materials with couple stresses. *Arch. Rational. Mech. Anal.*, vol. 11, no.1, pp. 385–414.
- Mindlin, R. D.** (1964): Micro-structure in linear elasticity. *Arch. Rational. Mech. Anal.*, vol. 16, no.1, pp. 51–78.
- Shu, J. Y.; King, W. E.; Fleck, N. A.** (1999): Finite elements for materials with strain gradient effects. *Int. J. Num. Meth. Eng.*, vol. 44, no. 3, pp. 373–391.
- Amanatidou, E.; Aravas, N.** (2002): Mixed finite element formulations of strain-gradient elasticity problems. *Comput. Methods Appl. Mech. Engrg.*, vol. 191, no. 15-16, pp. 1723–1751.
- Zervos, A.** (2008): Finite elements for elasticity with microstructure and gradient elasticity. *Int. J. Num. Meth. Eng.*, vol. 73, no. 4, pp. 564–595.
- Belytschko, T.; Krongauz, Y.; Organ, D.; Fleming, M.; Krysl, P.** (1996): Meshless methods: an overview and recent developments. *Comput. Methods Appl. Mech. Engrg.*, vol. 139, no. 1-4, pp. 3–47.
- Atluri, S. N.** (2004): *The Meshless Method (MLPG) for Domain & BIE Discretizations*. Tech. Science Press.
- Pamin, J.; Askes, H.; Borst, R.** (2003): Two gradient plasticity theories discretized with the element-free Galerkin method. *Comput. Methods Appl. Mech. Engrg.*, vol. 192, no. 20-21, pp. 2377–2403.
- Tang, Z.; Shen, S.; Atluri, S. N.** (2003): Analysis of materials with strain-gradient effects: a meshless local Petrov-Galerkin (MLPG) approach with nodal displacement only. *CMES: Computer Modeling in Engineering & Sciences*, vol. 4, no.1, pp. 177–196.

Sukumar, N.; Moran, B.; Semenov, A. Y.; Belikov, V. V. (2001): Natural neighbour Galerkin methods. *Int. J. Num. Meth. Eng.*, vol. 50, no.1, pp. 1–27.

Onate, E.; Zarate, F. (2000): Rotation-free triangular plate and shell elements. *Int. J. Num. Meth. Eng.*, vol. 47, no. 1, pp. 557–603.

Liu, G. R.; Nguyen, T. T.; Dai, K. Y.; Lam, K. Y. (2007): Theoretical aspects of the smoothed finite element method (SFEM). *Int. J. Num. Meth. Eng.*, vol. 71, no. 8, pp. 902–930.

Liu, G. R. (2008): A generalized gradient smoothing technique and the smoothed bilinear form for Galerkin formulation of a wide class of computational methods. *Int. J. Comput. Meth.* vol. 5, no. 2, pp. 199–236.

Sukumar, N.; Moran, B.; Belytschko, T. (1998): The natural element method in solid mechanics. *Int. J. Num. Meth. Eng.*, vol. 43, no. 5, pp. 839–887.

Belikov, V. V.; Semenov, A. Y. (2000): Non-Sibsonian interpolation on arbitrary system of points in Euclidean space and adaptive isolines generation. *Appl. Num. Math.*, vol. 32, no. 4, pp. 371–387.

Sukumar, N.; Moran, B. (1999): C^1 natural neighbor interpolant for partial differential equations. *Numer. Meth. Part. Diff. Eqn.*, vol. 15, no.4, pp. 417–447.

Babuska, I.; Melenk, J. M. (1997): The partition of unity method. *Int. J. Num. Meth. Eng.*, vol. 40, no.4, pp. 727–758.

Duarte, C. A.; Babuska, I.; Oden, J. T. (2000): Generalized finite element methods for three-dimensional structural mechanics problems. *Comput. Struct.*, vol. 77, no. 2, pp. 215–232.

Fan, S. C.; Liu, X.; Lee, C. K. (2004): Enriched partition-of-unity finite element method for stress intensity factors at crack tips. *Comput. Struct.*, vol. 82, no. 4-5, pp. 445–461.

Wells, G. N.; Sluys, L. J.; De Borst, R. (2002): A p-adaptive scheme for overcoming volumetric locking during plastic flow. *Comput. Methods Appl. Mech. Engrg.*, vol. 191, no. 29-30, pp. 3153–3164.

Gonzalez, D.; Cueto, E.; Doblare, M. (2004): Volumetric locking in natural neighbour Galerkin methods. *Int. J. Num. Meth. Eng.*, vol. 61, no. 4, pp. 611–632.

Yoo, J. W.; Moran, B.; Chen, J. S. (2004): Stabilized conforming nodal integration in the natural-element method. *Int. J. Num. Meth. Eng.*, vol. 60, no. 5, pp. 861–890.

Cordes, L. W.; Moran, B. (1996): Treatment of material discontinuity in the Element-free Galerkin method. *Comput. Methods Appl. Mech. Engrg.*, vol. 139, no. 1-4, pp. 75–89.

Yang, F.; Chong, A. C. M.; Lam, D. C. C.; Tong, P. (2002): Couple stress based strain gradient theory for elasticity. *Int. J. Solids Struct.*, vol. 39, no.10, pp. 2731–2743.